Available online at www.sciencedirect.com
SCIENCE DIRECT
Journal of Catalysis 232 (2005) 68–79
JOURNAL OF CATALYSIS
www.elsevier.com/locate/jcat

Mechanistic study of the influence of surface acidity on lean NO_2 reduction by propane in HZSM-5

Hanna Härelind Ingelsten [a,b,*], Dongmei Zhao [a,c], Anders Palmqvist [a,b], Magnus Skoglundh [a,b]

[a] *Competence Centre for Catalysis, Chalmers University of Technology, SE-412 96 Göteborg, Sweden*
[b] *Applied Surface Chemistry, Chalmers University of Technology, SE-412 96 Göteborg, Sweden*
[c] *Department of Chemistry, Göteborg University, SE-412 96 Göteborg, Sweden*

Received 22 December 2004; revised 24 February 2005; accepted 28 February 2005

Available online 7 April 2005

Abstract

This study focuses on the mechanism of lean NO_x reduction by propane, over acidic zeolites (HZSM-5), and the influence of surface acidity. In situ FTIR measurements of ammonia adsorption indicate a higher number of Brønsted acid sites for a sample with a low SiO_2/Al_2O_3 ratio. The activity for NO_x reduction and the selectivity for N_2 formation correlate well with the Brønsted acidity. Step-response experiments with NO_2 and propane show the formation of surface-bound NO^+, isocyanate, unsaturated hydrocarbons, and amine species. Formation of the latter two seems to be closely related to the Brønsted acidity. In the NO_2 reaction with propane, the NO^+ species seem to play a vital role, probably reacting with carbenium ions (from propane cracking) to form isocyanates, which may be hydrolysed to amine species. Step-response experiments with isopropylamine and NO_2 indicate a fast reaction, where the amine and NO^+ species react over Brønsted acid sites. Hence, amine species are possible reaction intermediates in the lean reduction of NO_2 by saturated hydrocarbons, such as propane, over HZSM-5.

Keywords: HZSM-5; Lean NO_x reduction; Propane; Isopropylamine; Surface acidity; FTIR

1. Introduction

Diesel and lean-burning engines are favourable engine concepts because of their relatively good fuel economy, which leads to less CO_2 formation. However, the lean environment in the exhaust obstructs the reduction of nitrogen oxides (NO_x) with the conventional three-way catalyst (TWC), since this technique requires stoichiometric conditions to achieve satisfactory NO_x abatement. This calls for more efficient techniques for lean NO_x reduction. Several solutions are possible, such as NO_x storage [1–3] and selective catalytic reduction with ammonia (NH_3-SCR) [4–6] or hydrocarbons (HC-SCR) [7–14] as the reducing agent for NO_x.

Platinum-based catalysts have been shown to be highly active towards NO_x reduction [15,16], with the use of HC-SCR. The high activity, unfortunately, is accompanied by low selectivity for N_2 formation [15]. In the presence of acidic groups on the surface of the support material, the N_2 selectivity can be enhanced [17]. Furthermore, it has been found that saturated hydrocarbons, such as propane, can be activated on the catalyst surface if the support material is modified to contain strong acidic sites [18,19] or by the introduction of surface sulphates [20–25]. Acke et al. studied the lean reduction of NO_x by C_3H_6, C_3H_8, NH_3, and HNCO over Pt supported on γ-Al_2O_3, ZSM-5, or SiC [7–11] and found that the NO_x reduction is affected by the platinum support material. Both the activity for NO_x reduction and the selectivity for N_2 formation were lowest for the samples supported on SiC, that is, the most inert support material. Previously we have investigated lean NO_x reduction, by propene or propane, over platinum supported on aluminum-silicates

* Corresponding author. Fax: +46 31 16 00 62.
E-mail address: hannahi@chem.chalmers.se (H.H. Ingelsten).

0021-9517/$ – see front matter
doi:10.1016/j.jcat.2005.02.022

[26] and over (Pt free) aluminum-silicates [27]. When platinum was present in the samples we found a strong connection between the Brønsted site density and the selectivity for N_2 formation [26], even though the relation to the activity for NO_x reduction was not as clear. However, for the aluminium-silicate samples we found a clear correlation between the amount of Brønsted acid sites and the NO_x reduction activity, for propane as the reducing agent [27]. Thus, previous results illustrate the important role of the support material for lean NO_x reduction and emphasise the connection between the activity for NO_x reduction, N_2 selectivity, and surface acidity.

Since NO_2 is more easily reduced than NO, one possible NO_x reduction route involves an initial oxidation of NO to NO_2. Some NO_x reduction systems, such as the dual pore system, utilise this concept, starting by selective oxidation of NO [28,29]. The subsequent NO_2 reduction step in the dual pore system occurs over acidic zeolites, where the acidity seems to be the key factor for the process to occur.

In this work we have focused on the continuous catalytic reduction of NO_2 by propane over acidic zeolites (HZSM-5) with varying SiO_2/Al_2O_3 ratio. The objective was to study the mechanism of lean NO_x reduction by propane and its correlation with the surface acidity.

2. Experimental

2.1. Catalyst preparation

The catalysts used in this study were HZSM-5 zeolites (Akzo Nobel Catalysts BV) with varying SiO_2/Al_2O_3 molar ratio (Table 1). To vary only the surface acidity, the catalytic samples are chosen to have similar textural properties, with the exception of the SiO_2/Al_2O_3 molar ratio. The zeolite powders were pressed into discs, which were ground and sieved to obtain a size fraction of 300 to 500 μm. The samples where then calcined in air at 500 °C for 1 h.

2.2. Activity and characterisation

2.2.1. NO_x reduction activity

The activity and selectivity for NO_x reduction with C_3H_8 were investigated in a vertical flow reactor (21 mm i.d., 58-cm-long quartz tube with a thin sintered quartz filter disc fused into the tube 28 cm from the upper end). The reactor was heated by a tubular furnace (controlled by Eurotherm 818S), and the temperature was measured with a thermocouple (K-type) located inside the reactor, 2 mm above the catalyst bed. Gases, He (99.9996%), O_2 (99.9996%), NO_2 (0.983% in He), and C_3H_8 (2% in He), were introduced via separate mass flow controllers. Reactant and product gases were analysed on-line. NO and NO_2 were determined with an Eco Physics, CLD 569 EL ht chemiluminescence analyser. An Agilent 6850 gas chromatograph fitted with a HP-PLOT Molesieve column and a thermal conductivity detector was used to quantify N_2. Water, CO_2, NO_x, and unreacted hydrocarbons were removed by a liquid nitrogen-cooled cold trap, located upstream of the gas chromatograph. CO, CO_2, and N_2O were measured by photoacoustic FTIR spectroscopy, with a Bruel & Kjaer Type 1301 analyser. Other possible nitrogen-containing reaction products, if present, were detected by the same technique. The catalyst samples were pretreated in 10% O_2 balanced with He (30 min at 500 °C), and the gas composition used in the experiments was 10% O_2, 1040 ppm NO_2, and 300 ppm C_3H_8, balanced with He to maintain a total gas flow rate of 1500 ml/min, corresponding to a space velocity of 50,000 h^{-1}. Steady-state measurements were performed at 650, 550, 450, and 350 °C.

Table 1
Textural properties of the HZSM-5 zeolites used in the experiments

	HZSM-5 40	HZSM-5 234	HZSM-5 569
Crystallinity (%)	95	98	100
SiO_2/Al_2O_3	39.7	234	569
Na_2O (wt%)	< 0.05	0.01	0.03
MiPV[a] (ml/g)	0.177	0.183	0.183
SA[b] (m^2/g)	405	407	377

[a] Micro pore volume.
[b] BET surface area.

2.2.2. FTIR spectroscopy

The in situ FTIR (Fourier transform infrared) spectroscopy measurements were carried out with a BioRad FTS 6000 spectrometer in diffuse reflectance (DRIFT) mode. The setup is described elsewhere [27,30]. The calcined zeolite samples were placed in the DRIFT cell. The gases, Ar (99.995%), O_2 (99.95%), NO_2 (5000 ppm in Ar), C_3H_8 (1% in Ar), and NH_3 (4% in Ar), were introduced via mass flow controllers (Bronkhorst Hi-Tech) to the DRIFT cell. The samples were initially pretreated in nitrogen dioxide and oxygen (1000 ppm NO_2 and 10% O_2, balanced with Ar, 500 °C, 40 min) followed by oxygen (10% O_2 in Ar, 500 °C, 1 h) and then evacuated in pure Ar (500 °C, 15 min) at a total flow rate of 300 ml/min (the flow rate was kept constant throughout the experiments). Background spectra (40 scans at a resolution of 1 cm^{-1}) were collected for each temperature, under Ar exposure. Fresh samples were used for all experiments.

Ammonia adsorption experiments were carried out at 450, 350, and 250 °C to distinguish the acidity of the zeolites. The samples were exposed to 1000 ppm NH_3 in Ar until saturation (about 10 min) and then flushed with pure Ar for 10 min. Spectra (20 scans at a resolution of 1 cm^{-1}) were taken continuously during the experiments.

Step-response experiments (with propane as a reducing agent) were performed for two of the samples, HZSM-5 40 at 450 and 350 °C and HZSM-5 234 at 450 °C. The experiment consisted of six sequences with different gas compositions, and spectra (five scans at a resolution of 1 cm^{-1}) where taken after 0, 20 s, and 1, 2, 3, 5, 7, 10, 15, and

20 min (or until saturation was reached) for each sequence. Sequence 1 started with a fresh sample (pretreated as mentioned above), and a mixture of 1000 ppm NO_2 and 10% O_2 (balanced with Ar) was introduced to the sample cell (at time 0 s). When saturation was reached the gas composition was changed and new spectra were collected. The subsequent sequences proceeded as follows:

Sequence 2 300 ppm propane was added (1000 ppm NO_2, 300 ppm C_3H_8, 10% O_2, balanced with Ar).
Sequence 3 The NO_2 was turned off (300 ppm C_3H_8, 10% O_2, balanced with Ar).
Sequence 4 The NO_2 was turned on (1000 ppm NO_2, 300 ppm C_3H_8, 10% O_2, balanced with Ar).
Sequence 5 The propane was turned off (1000 ppm NO_2, 10% O_2, balanced with Ar).
Sequence 6 The propane was turned on (1000 ppm NO_2, 300 ppm C_3H_8, 10% O_2, balanced with Ar).

For the HZSM-5 40 sample, step-response experiments were also performed, with isopropylamine as the reducing agent. The background spectra were collected under reaction conditions (20 scans at a resolution of 4 cm^{-1}), and the difference spectra were recorded, when either NO_2 or isopropylamine was turned off and on, at 450, 350, and 250 °C, respectively (1 scan/s, 4 cm^{-1} resolution). The experimental setup was the same as that for the previous experiments, with the exception of one additional Ar flow, which was saturated with isopropylamine before the reaction cell. In addition, spectra were taken (five scans at a resolution of 1 cm^{-1}) when isopropylamine was pre-adsorbed on the sample, and a mixture of 1000 ppm NO_2 and 10% O_2, balanced with Ar, was subsequently introduced. Background spectra, 40 scans at a resolution of 1 cm^{-1}, were collected under Ar exposure directly after the pretreatment.

3. Results

3.1. Acidity characterisation

The background spectrum for the HZSM-5 40 sample (collected under Ar) shows absorption peaks at 3737 and 3600 cm^{-1}, which are assigned to OH stretching vibrations originating from silanol groups (Si–OH) and Si(OH)Al bridging hydroxyl groups, respectively [6,31–37] (Fig. 1). The latter peak (3600 cm^{-1}) is typical for Brønsted acid sites in zeolites. This peak is significantly weaker for the HZSM-5 234 sample and is absent for the HZSM-5 569 sample. The background spectra are indicative of the differences in acidity between the different samples, where the HZSM-5 40 sample contains significant amounts of Brønsted acid sites in the zeolite framework.

To further investigate the acidity of the samples, FTIR spectra were recorded during ammonia exposure at 450, 350, and 250 °C; the results are shown in Fig. 2. For the HZSM-5

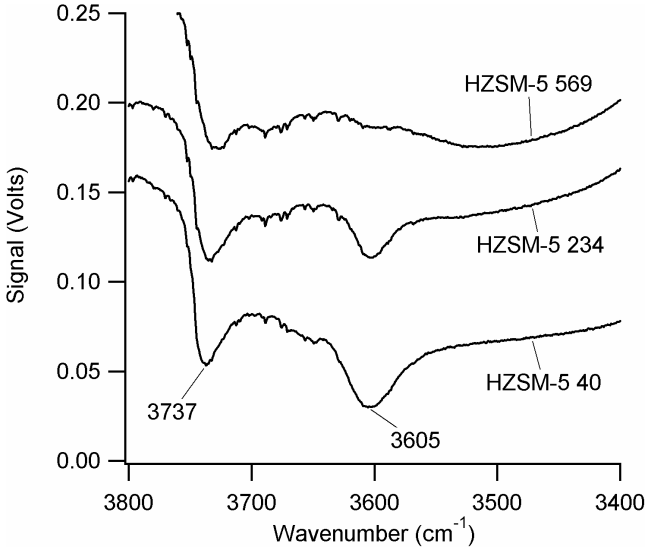

Fig. 1. FTIR spectra collected at steady-state during Ar flow at 250 °C. The measured signals of the baselines are separated by −0.02, 0.03 and 0.1 V, respectively.

40 sample (steady state, 250 °C) peaks at 3374, 3283, and 1483 cm^{-1} appear, which are attributed to asymmetric and symmetric NH stretching and bending vibrations of NH_4^+ at the Brønsted acid sites [6,34,38,39]. The origin of the 1483 cm^{-1} peak is somewhat uncertain, however, since there are possible bands in this region (below 2000 cm^{-1}) connected to perturbed vibration frequencies of the zeolite framework [6,37,40]. The presence of NH_4^+ species at the Brønsted acid sites is also strongly supported by the pronounced negative peak that appears at 3607 cm^{-1}, which is assigned to OH stretching vibrations of the Brønsted acid sites [6,34,39]. Bands at 3248, 3208, and 2736 cm^{-1} are also observed that most likely are due to NH stretching vibrations of NH_4^+ [6,41] and in the latter case to weakly bound NH_3 [6]. During the ammonia adsorption the presence of trace amounts of water cannot be excluded, and the broad feature observed in the region of 3500–2200 cm^{-1} may be related to OH stretching vibrations of water present at the Lewis acid sites in the sample [6,37]. Increasing the temperature results in an overall decrease in the peak heights. The peaks related to NH_4^+ species at Brønsted acid sites (3374, 3283, and 1483 cm^{-1}) and OH stretching vibrations of Brønsted acid sites (3607 cm^{-1}) decrease slightly with increasing temperature.

The intensities of the peaks in the NH stretching region (3400–3200 cm^{-1}), compared with the HZSM-5 40 sample, are significantly lower for the HZSM-5 234 sample and absent for the HZSM-5 569 sample. Furthermore, the peak originating from OH stretching vibrations at 3607 cm^{-1} (Brønsted acid sites) is significantly weaker for the HZSM-5 234 sample and negligible for the HZSM-5 569 sample.

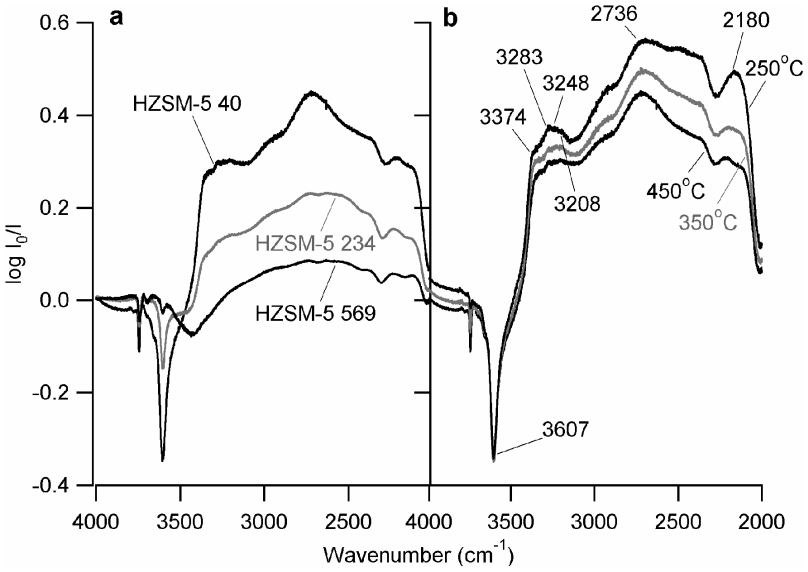

Fig. 2. FTIR spectra collected at steady-state conditions during a flow of 1000 ppm NH_3 in Ar (a) at 450 °C over HZSM-5 40, HZSM-5 234, and HZSM-5 569, respectively, and (b) at 250, 350, and 450 °C over HZSM-5 40.

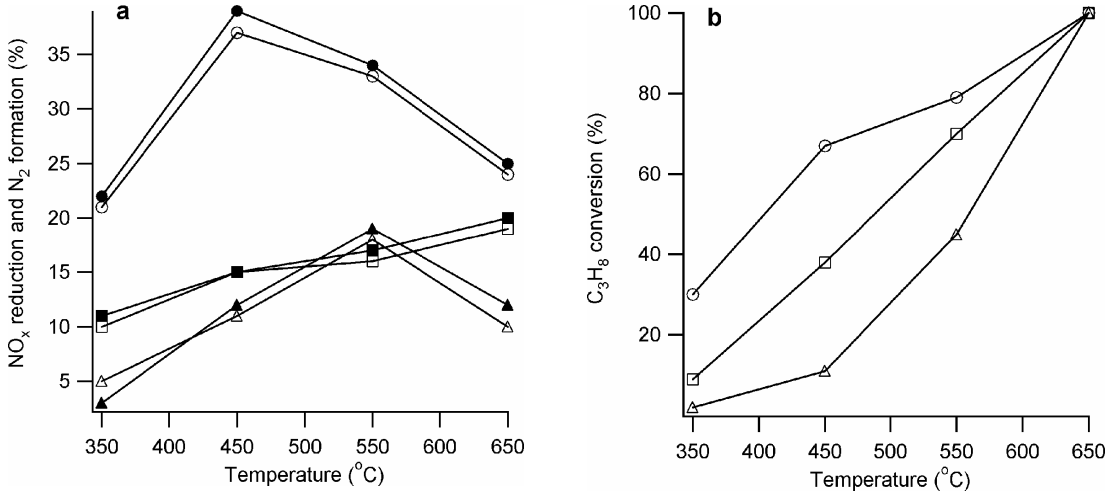

Fig. 3. (a) N_2 formation (percentage of the sum of all N-containing species in the outlet gas flow), designated by open symbols and NO_x reduction (percentage of the sum of all N-containing species in the outlet gas flow) designated by filled symbols, during steady-state NO_2 reduction experiments in oxygen excess, using propane as reducing agent: circle, HZSM-5 40; square, HZSM-5 234; and triangle, HZSM-5 569. (b) C_3H_8 consumption (percentage of the sum of all C-containing species in the outlet gas flow) during steady-state NO_2 reduction experiments in oxygen excess, using propane as reducing agent: circle, HZSM-5 40; square, HZSM-5 234; and triangle, HZSM-5 569.

3.2. Activity studies

Fig. 3 shows the NO_x reduction, the N_2 formation (in percentage of the sum of all N-containing species in the outlet gas flow), and the C_3H_8 consumption (in percentage of the sum of all C-containing species in the outlet gas flow) for the different samples as a function of the reactor temperature. The highest activities for NO_x reduction and the formation of N_2 are obtained with the HZSM-5 40 sample at 450 °C, followed, in decreasing order of activity, by HZSM-5 234 and HZSM-5 569. For the latter two samples the maximum N_2 formation is achieved at higher temperatures, 550 °C and above. The formation of N_2O is low for all of the samples and does not exceed 1.5% at any temperature.

The influence of mass transfer limitations on the reduction of NO_x is considered by estimation of the Weiszs modulus (see Appendix A), and the results show that the catalytic reaction is likely not influenced by mass transport limitations.

3.3. Mechanistic studies

The results from the step-response experiments, performed with the in situ FTIR equipment, are presented in Figs. 4–6 and 8. Below 2000 cm^{-1} the background noise

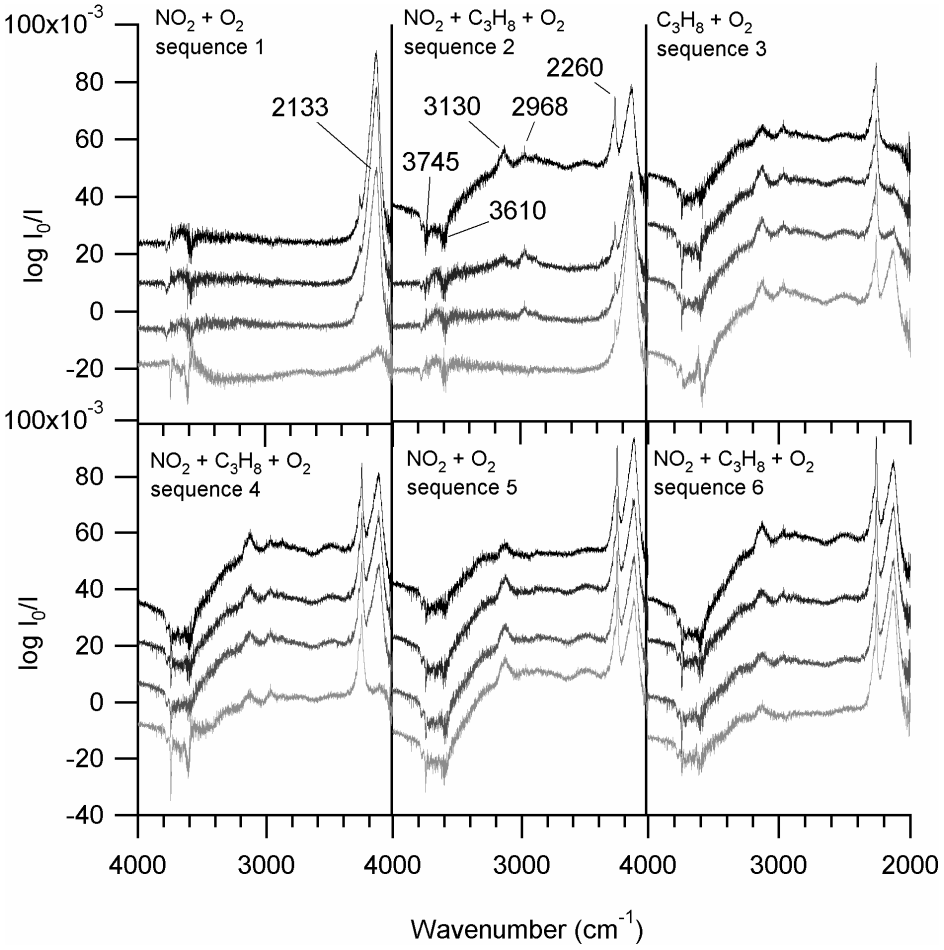

Fig. 4. Step-response experiments at 450 °C, over HZSM-5 40 zeolite, using propane as the reducing agent. Light grey corresponds to direct after the gas switch and time is then increased until steady-state is reached, which is illustrated with black. Sequence 1: 1000 ppm NO_2, 10% O_2 in Ar; sequence 2: 1000 ppm NO_2, 300 ppm C_3H_8, 10% O_2 in Ar; sequence 3: 300 ppm C_3H_8, 10% O_2 in Ar; sequence 4: 1000 ppm NO_2, 300 ppm C_3H_8, 10% O_2 in Ar; sequence 5: 1000 ppm NO_2, 10% O_2 in Ar; sequence 6: 1000 ppm NO_2, 300 ppm C_3H_8, 10% O_2 in Ar.

level is significant, which is probably related to perturbed vibration frequencies of the zeolite framework [6,37,40], which make peak observation and assignment difficult in this region.

3.3.1. *Reduction of NO_2 by propane over HZSM-5 40*

Step-response experiments for HZSM-5 40, with propane as the reducing agent, are shown in Figs. 4 and 5. During the first sequence (1000 ppm NO_2 and 10% O_2), one peak is observed at 2133 cm^{-1} (for both 450 and 350 °C). At 350 °C this peak increases during the first minute of exposure, after which it gradually decreases and reaches a steady-state level after about 20 min, which has also been observed by Xin et al. [42]. According to Hadjiivanov and co-workers [31], the 2133 cm^{-1} peak corresponds to NO^+ species present at the Brønsted acid sites in the zeolite. Since weak negative peaks are observed around 3610 and 3745 cm^{-1}, which are assigned to OH stretching vibrations originating from Brønsted acid sites and silanol groups, respectively [6,31–37], it is probable that the NO^+ species are present at the Brønsted acid sites. When propane is brought into contact with the sample (sequence 2: 1000 ppm NO_2, 300 ppm C_3H_8, and 10% O_2), several peaks appear. At 450 °C the NO^+ peak decreases slightly with time, and a peak at 2260 cm^{-1} with a small shoulder at 2275 cm^{-1} appears. These peaks are most probably due, respectively, to isocyanate (–NCO) species bound to Al and Si in the zeolite framework [35,43–50] and/or nitrile species [35,43,46,47,51]. At 350 °C the 2260 cm^{-1} peak is present only as a small shoulder on the NO^+ peak, and there is no sign of the shoulder at 2275 cm^{-1}. Several peaks are observed in the 3000–2800 cm^{-1} region, which most likely can be assigned to CH stretching vibrations [35,42,47]. A peak at 2968 cm^{-1} in particular can be attributed to adsorbed and/or gas-phase propane [52]. These peaks (3000–2800 cm^{-1}) appear already after ca. 20 s and seem to be constant throughout the sequence (for both temperatures). After about 1 min, a peak around 3130 cm^{-1} starts to grow (450 °C) and increases until saturation is reached. This peak may be due to CH stretching vibrations of unsaturated hydrocarbons [46,47]. For the lower temperature (350 °C) this peak is significantly weaker. In the NH stretching region of 3400–3200 cm^{-1} [35,46,47,53,54] a

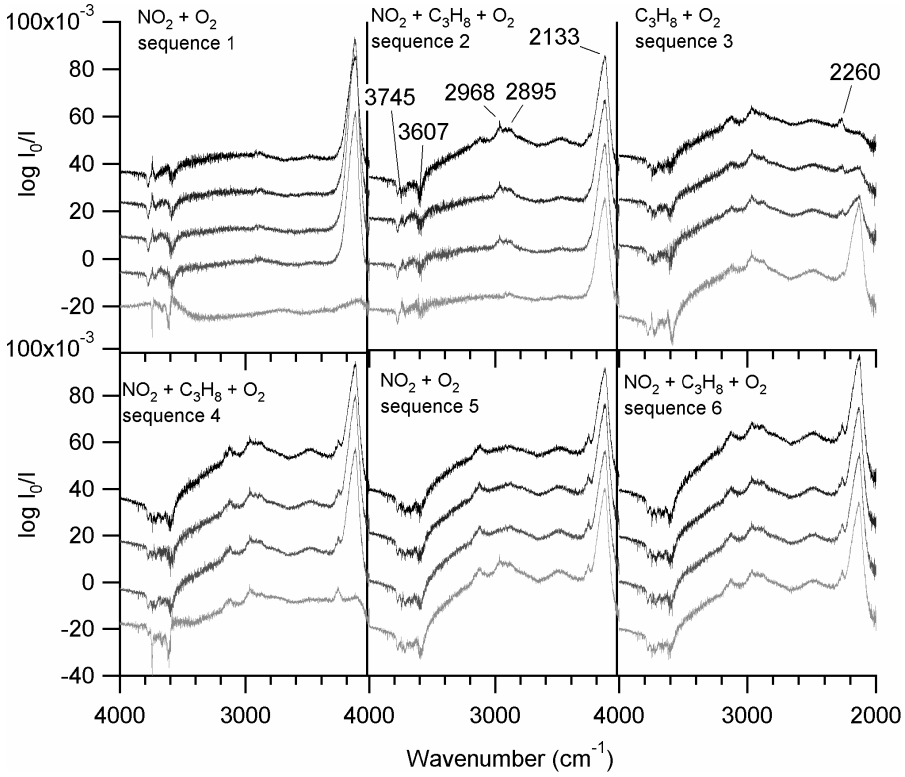

Fig. 5. Step-response experiments at 350 °C, over HZSM-5 40 zeolite, using propane as the reducing agent. Light grey corresponds to direct after the gas switch and time is then increased until steady-state is reached, which is illustrated with black. Sequence 1: 1000 ppm NO_2, 10% O_2 in Ar; sequence 2: 1000 ppm NO_2, 300 ppm C_3H_8, 10% O_2 in Ar; sequence 3: 300 ppm C_3H_8, 10% O_2 in Ar; sequence 4: 1000 ppm NO_2, 300 ppm C_3H_8, 10% O_2 in Ar; sequence 5: 1000 ppm NO_2, 10% O_2 in Ar; sequence 6: 1000 ppm NO_2, 300 ppm C_3H_8, 10% O_2 in Ar.

small shoulder is observed at 450 °C, which possibly can be attributed to amine species. The negative peak around 3610 cm^{-1} gradually becomes more negative during the sequence with propane (more negative for 450 than for 350 °C). This is indicative of blocking of the Brønsted acid sites by adsorbed species, most likely hydrocarbons. In sequence 3, when NO_2 is turned off (300 ppm propane and 10% O_2), the NO^+ peak rapidly disappears and the –NCO peak becomes less intense. The 3610 cm^{-1} peak is constant. In the CH vibration region the magnitude of the peaks decreases, but the relative heights of the separate peaks are constant. This may be due to less water formation, since NO_2 is a stronger oxidising agent than O_2. The OH stretching vibrations of water, hydrogen-bonded to Lewis acid sites, appear in the 3500–2200 cm^{-1} region [6,37]. The changes in the spectra are similar for the two temperatures, except for the NH stretching region, where a shoulder is observed at 450 °C, whereas there are no signs of NH vibrations at 350 °C. When NO_2 is turned on again (sequence 4), the NO^+ peak develops and the –NCO peak increases slightly. The signal in the CH stretching region increases (with the relative peak heights constant), likely because of increased water formation. The shoulder in the NH region becomes more pronounced (450 °C), and the 3610 cm^{-1} peak is constant. During sequence 5 (propane is turned off) the NO^+ peak is constant at 450 °C but decreases slightly at 350 °C. The isocyanate peak decreases but is still significant at steady state (for both temperatures). In the CH region the peaks decrease markedly at 350 °C and disappear at 450 °C, and the propane peak disappears completely (for both temperatures). The peak at 3130 cm^{-1} decreases but does not disappear, and the 3610 cm^{-1} peak becomes less negative. In the final sequence (sequence 6) propane is turned on again, and the bands in the CH-region, including the propane peak and the peak at 3130 cm^{-1}, increase. The 3610 cm^{-1} peak gradually becomes more negative, the isocyanate peak increases, and the shoulder in the NH-region, which appears at 450 °C, becomes more distinct.

Sequences 2 and 6 should be similar since, in both cases, propane is turned on after a sequence with only NO_2 and oxygen. There are some differences in the results, however, which may be explained by the presence of C-containing species on the surface before the sixth sequence starts. At 450 °C the –NCO peak is higher than the NO^+ peak in sequence 6; however, in sequence 2 the NO^+ peak is higher than the –NCO peak. Moreover, the shoulder in the NH region (450 °C) is more pronounced in sequence 6 than in sequence 2. The shoulder at 2260 cm^{-1}, which appears in sequence 2 at 350 °C, becomes a small peak in sequence 6, and the 3130 cm^{-1} peak is increased slightly in sequence 6 compared with sequence 2.

The differences between the two temperatures indicate more interaction on the surface at the higher temperature (450 °C). The unsaturated hydrocarbon peak seems more

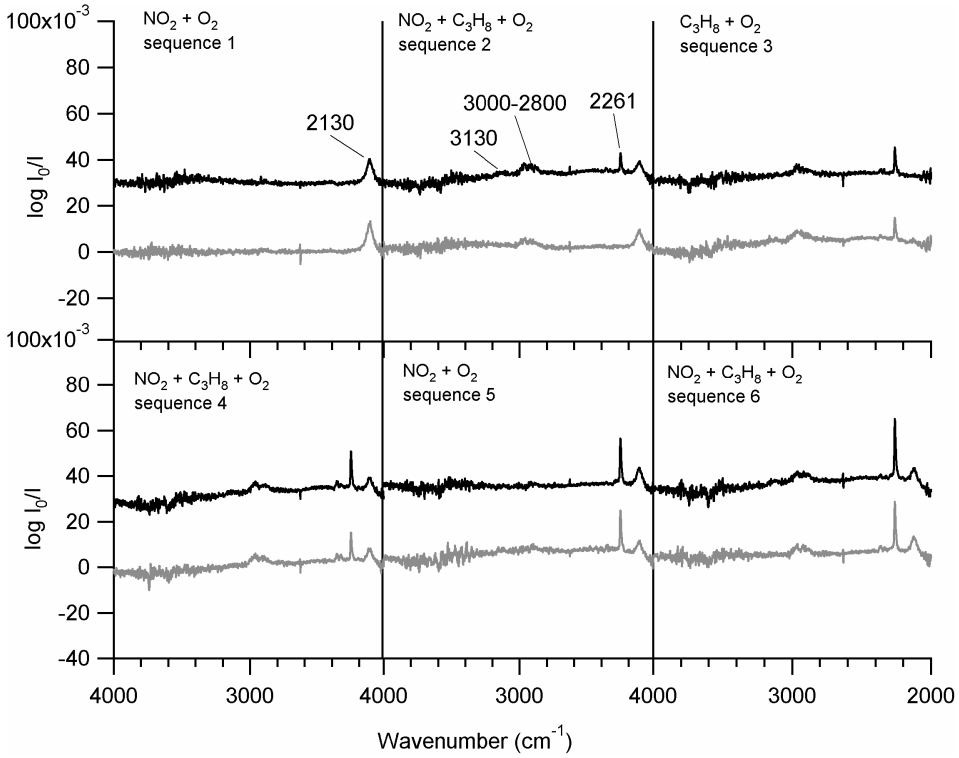

Fig. 6. Step-response experiments at 450 °C, over HZSM-5 234 zeolite, using propane as the reducing agent. Light grey corresponds to direct after the gas switch and time is then increased until steady-state is reached, which is illustrated with black. Sequence 1: 1000 ppm NO_2, 10% O_2 in Ar; sequence 2: 1000 ppm NO_2, 300 ppm C_3H_8, 10% O_2 in Ar; sequence 3: 300 ppm C_3H_8, 10% O_2 in Ar; sequence 4: 1000 ppm NO_2, 300 ppm C_3H_8, 10% O_2 in Ar; sequence 5: 1000 ppm NO_2, 10% O_2 in Ar; sequence 6: 1000 ppm NO_2, 300 ppm C_3H_8, 10% O_2 in Ar.

intense, and the Brønsted peak is more negative for this temperature. The isocyanate peak is visible only as a small shoulder, which develops to a small peak at 350 °C, whereas at 450 °C this peak is significantly more pronounced. Furthermore, there are no indications of NH vibrations at 350 °C. At 450 °C, on the other hand, a small shoulder is observed in the NH region. These results correlate well with the activity study, where the NO_x reduction activity is found to be higher at 450 than at 350 °C.

3.3.2. Reduction of NO_2 by propane over HZSM-5 234

In Fig. 6 the results from the step-response experiments with propane at 450 °C over the HZSM-5 234 sample can be seen. The first sequence (with only NO_2 and oxygen) is similar to the experiment for HZSM-5 40, that is, one peak at around 2130 cm^{-1} is observed. When propane is turned on (sequence 2), peaks at 2261, 3000–2800, and 3130 cm^{-1} evolve. The –NCO peak is relatively high compared with the NO^+ peak. In sequence 3, NO_2 is turned off, the NO^+ peak gradually disappears, and the isocyanate peak seems constant. Turning on the NO_2 again (sequence 4) results in a developing NO^+ peak and a small increase in intensity of the peaks in the CH region. In sequence 5 the propane is turned off and the CH stretching vibrations gradually disappear. When the propane is turned on (sequence 6) these peaks start to grow again. The signal in the OH region is very noisy in these experiments; however, in the last sequence (sequence 6) some small negative peaks can be observed around 3610 and 3745 cm^{-1}, indicating blocking of OH sites.

An overall observation for this sample is that the total amount of adsorbates is much less than for the HZSM-5 40 sample. In particular, the 3130 cm^{-1} peak and the peaks in the OH region are significantly less intense or do not appear at all for some of the sequences. An interesting observation is that the –NCO peak increases (to approximately three times the initial size) during the entire experiment. During this experiment there are no signs of NH stretching vibrations, which are observed at this temperature for the HZSM-5 40 sample.

3.3.3. Reduction of NO_2 by isopropylamine over HZSM-5 40

Since there are signs of NH stretching vibrations during the step-response experiments over HZSM-5 40, and the presence of amine intermediates in the HC-SCR reaction is debated in the literature [45,47,53–57], step-response experiments with isopropylamine as the reducing agent for NO_2 are performed. The results are summarised in Figs. 7 and 8.

Fig. 7 shows the reaction of pre-adsorbed isopropylamine with NO_2 and O_2 (at 500 °C). Initially, before the NO_2 and O_2 are turned on, four main groups of peaks can be observed. The peaks at 2786, 2910, 2942, and 2987 cm^{-1} are attributed to (saturated) CH stretching vibrations [35,42,46,47], and

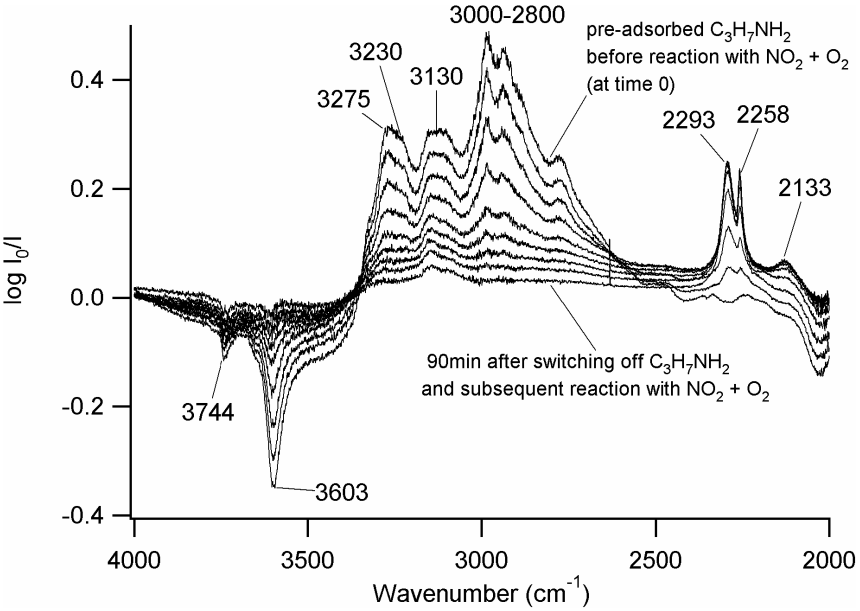

Fig. 7. Reaction of pre-adsorbed isopropylamine with 1000 ppm NO_2 and 10% O_2 (balanced with Ar) at 500 °C. The time separation between the spectra is approximately 10 min.

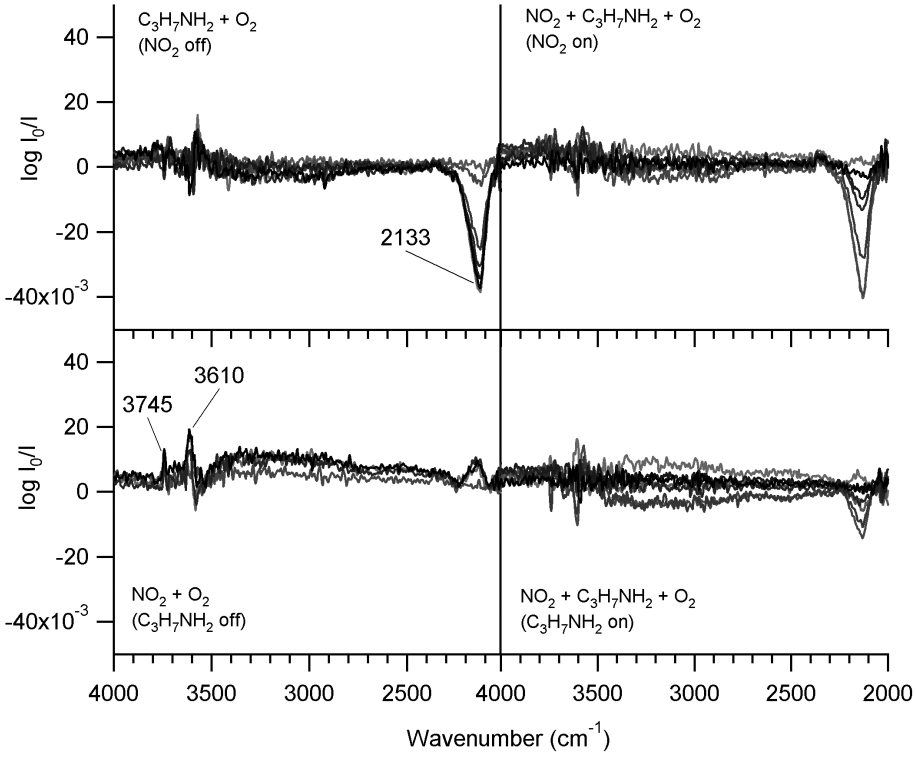

Fig. 8. Step-response experiments at 450 °C, over HZSM-5 40 zeolite, using isopropylamine as the reducing agent. Light grey corresponds to direct after the gas switch and time is then increased until steady-state is reached, which is illustrated with black.

the peak at 3130 cm^{-1} originates most likely from (unsaturated) CH vibrations [46,47]. One peak at 3275 cm^{-1}, with a shoulder around 3230 cm^{-1}, is probably due to NH stretching vibrations from amine species [35,46,47,53,54], and the negative peaks at 3603 and 3745 cm^{-1} indicate blocking of the Brønsted acid sites and silanol groups [6,31–37], presumably by hydrocarbon and/or amine species, respectively. When NO_2 and oxygen are introduced into the sample cell, the intensities of the CH stretching vibrations and the NH stretching region decrease and eventually disappear. The OH peaks gradually become less negative, approaching the zero level; that is, the species that block the sites disappear. Peaks at 2258, 2293, and 2133 cm^{-1} start to grow. The latter is likely due to NO^+ species [31] formed on the surface as the

isopropylamine is consumed. The peak at 2258 cm^{-1} probably relates to isocyanate species, and the peak at 2293 cm^{-1}, to CO_2 (in gas phase) [58], which is formed during the reaction between NO_2 and isopropylamine.

Step-response experiments with isopropylamine as a reducing agent are shown in Fig. 8. The background spectra are collected at reaction conditions (for each temperature). Nitrogen dioxide and isopropylamine are alternatively turned on and off. Spectra are recorded every second during this process. When NO_2 is turned off at 450 °C, a negative peak develops at 2133 cm^{-1}, corresponding to the disappearance of NO^+ species. The NO^+ peak returns to the zero level (complete reaction) again when NO_2 is turned on. Isopropylamine is then switched off and positive peaks appear at 2133, 3610, and 3745 cm^{-1}. These peaks are related to the formation of NO^+ species and formation and/or unblocking of Brønsted acid sites and silanol groups at the sample surface, respectively. It is likely that the Brønsted acid sites are occupied by hydrocarbon and/or amine species, which are consumed in the reaction when the isopropylamine is turned off. Isopropylamine is then turned on again and a negative peak at 2133 cm^{-1} is initially formed together with negative peaks in the OH region. The negative peak at 2133 cm^{-1} reaches a maximum value (in less than 1 min), after which it decreases in magnitude and eventually reaches the zero level (complete reaction). The results from the step-response experiments at 350 and 250 °C are similar. However, the reaction seems to proceed more slowly at the lower temperatures, and turning off the isopropylamine results in negligible changes (compared with the complete reaction).

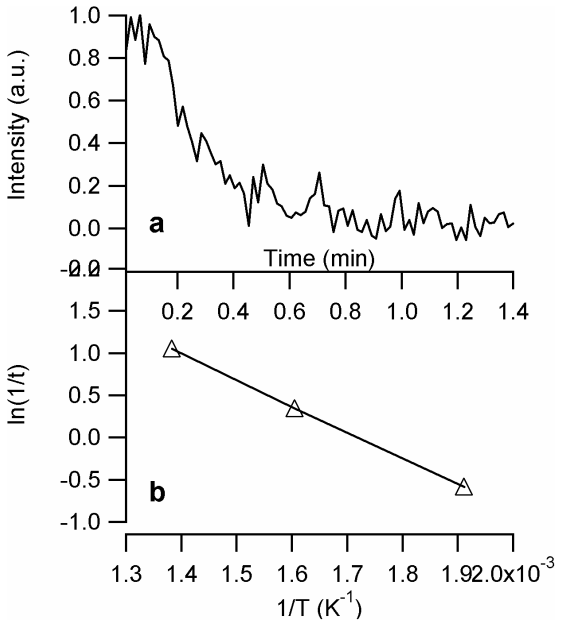

Fig. 9. Intensity change during isopropylamine reaction when NO_2 is turned on. (a) Intensity of the NO^+ peak (2133 cm^{-1}) vs time (min) at 450 °C and (b) $\ln(1/t)$ vs $1/T$, where t is the time consumed for the intensity to decrease from 90 to 10%. The slope corresponds to the activation energy, E_a.

The intensity of the NO^+ peak is monitored as a function of time (Fig. 9), and the change is used to calculate the apparent activation energy (E_a) for the reaction, from the Arrhenius equation,

$$k = Ae^{-E_a/RT}, \quad (1)$$

where k is the rate constant, A is the pre-exponential factor, E_a is the activation energy, R is the gas constant, and T is the temperature. With this expression the apparent activation energy (E_a) for the reaction, when NO_2 is turned on, is found to equal approximately 25 kJ/mol. The corresponding value for E_a, when isopropylamine is turned on, is ca. 10 kJ/mol. These activation energies are relatively low, which is also expected, since the reaction seems to proceed quickly.

4. Discussion

In previous studies of lean NO_x reduction by hydrocarbons over Pt/aluminum-silicates [26] and over aluminum-silicates [27], we have found a clear correlation between the activity for NO_x reduction and the Brønsted-site density, as well as between the N_2 selectivity and the Brønsted-site density. In the present work we focus on the mechanism for NO_x reduction by saturated hydrocarbons and the influence of the acidity of the catalyst samples.

The ammonia adsorption experiments with FTIR indicate strong Brønsted acid sites for the sample with low SiO_2/Al_2O_3 ratio, whereas the samples with a high SiO_2/Al_2O_3 ratio show low or negligible amounts of Brønsted acid sites. The acidity is found to correlate well with the NO_x reduction activity and with the N_2 formation, which is highest for the HZSM-5 40 sample.

To study the lean reduction of NO_x in more detail, step-response experiments with FTIR, where NO_2 and propane are turned off and on, are performed over two of the samples (HZSM-5 40 and HZSM-5 234). When the samples are exposed to NO_2, NO^+ species are formed, likely on Brønsted acid sites. The possible formation of surface-bound nitrates (NO_3^-) and nitrites (NO_2^-), which should be indicated by IR absorption bands in the region of 1650–1000 cm^{-1}, has not been studied in the present work because of disturbances related to perturbed vibrations of the zeolite framework (below 2000 cm^{-1}). However, nitrates are formed mainly on basic oxides; for instance, Svedberg and co-workers [59] investigated the ability to store NO_x (as nitrates) for several materials and found that the NO_x storage capacity increased with increasing basicity of the support material. For the most acidic sample investigated (an aluminium-silicate sample), the amounts of stored NO_x at temperatures above 300 °C were negligible. Furthermore, Hadjiivanov et al. [31] have performed NO + O_2 adsorption on HZSM-5 zeolites, and they state that the NO^+ species is the only stable NO_x surface species on HZSM-5. Hence we conclude that the formation of nitrates on the acidic zeolites used in this study is less likely.

For both samples (HZSM-5 40 and HZSM-5 234) isocyanate (and/or nitrile) species are formed when both NO_2 and propane are present in the feed gas. Especially for the less acidic sample (HZSM-5 234), isocyanate species seem to be accumulated rather than consumed. However, for the more acidic sample (HZSM-5 40) these species seem to be accumulated but are partly consumed when either NO_2 or propane is turned off. This accumulation of isocyanate species is probably related to the water formation that occurs during the reaction. The NCO species are likely hydrolysed to amine species [55], and when all water is consumed the hydrolysis will decrease and eventually stop. Since the propane conversion and the NO_x reduction are higher for the HZSM-5 40 sample (compared with the less acidic sample), it is likely that more water is also formed over this sample, and hence the accumulation of NCO species is less for this sample compared with the HZSM-5 234 sample. During the sequences with propane, CH vibrations probably related to gas-phase propane and/or loosely bound hydrocarbons are observed. After ca. 1 min (of propane present in the feed gas), a peak, which can be due to unsaturated hydrocarbons on the surface, appears for the more acidic sample. This peak grows as the negative OH vibration peak, typical for Brønsted acid sites in zeolites, becomes more negative. Hence, it seems likely that the unsaturated hydrocarbons are formed on the Brønsted acid sites, since the OH peak becomes more negative when the unsaturated hydrocarbon peak increases, that is, the Brønsted acid sites are blocked. This is further illustrated by the fact that this peak is small or negligible for the HZSM-5 234 sample (which contains significantly lower amounts of Brønsted acid sites). From the hydrocarbon cracking literature it is well known that Brønsted acid sites catalyse the cracking of hydrocarbons. For instance, Jentoft et al. [60] describe this phenomenon and suggest, as one possible route, that strong proton–donor sites of the catalyst (i.e., Brønsted acid sites) can protonate the alkane to form alkanium ions, which subsequently collapse to form carbenium ions and then further react to form alkenes. From these results it is evident that the surface acidity plays an important role for the NO_2 reduction by propane over this type of catalyst sample. The Brønsted acid sites seem to be indispensable for the activation of the propane (i.e., to form some kind of carbenium ions), so that further reactions can proceed.

The step-response experiments also show indications of a shoulder in the NH region for the HZSM-5 40 sample at 450 °C. The shoulder is more pronounced when both NO_2 and propane are present in the feed gas, but is also observed when either NO_2 or propane is turned off. The latter may be related to accumulation of isocyanate (and/or nitrile) species, which can be readily hydrolysed to amine species [11,48,50,61,62]. For the less acidic sample there are no signs of NH vibrations. Consequently, the NH vibrations also seem to correlate with the Brønsted acidity.

To further investigate the surface reactions, isopropylamine is used as the reducing agent for NO_x, and the results indicate a rapid reaction between the isopropylamine and NO_x species. In this process the NO^+ species seem to play a vital role. When the NO_2 is switched off (in the step-response experiments), a negative peak corresponding to removal of the NO^+ species occurs. Similarly, when the isopropylamine is turned on, the negative NO^+ peak immediately develops, which after a short period of time decreases in magnitude and approaches the zero level (reaction conditions). When the isopropylamine is switched off (at 450 °C) positive peaks at 2133, 3610, and 3745 cm^{-1} become visible. These peaks are probably related to the formation of NO^+ species on the surface and unblocking of Brønsted acid sites, respectively. During reaction conditions it is conceivable that hydrocarbon and/or amine species, originating from the isopropylamine, are present at the Brønsted acid sites. These species are consumed in the reaction, and the Brønsted sites appear as a positive peak at the same time that the NO^+ species start to accumulate on the surface. Hence, it seems likely that the NO^+ species react with isopropylamine-derived species and that the reaction proceeds over Brønsted acid sites in the zeolite.

5. Conclusions

The reactants are most likely adsorbed surface species for which the functional group (isocyanate, amine, etc.) is the key in the reaction. The exact nature of the adsorbed molecule is less certain and most probably also of minor importance for the overall reaction pathway. We can conclude that the propane is likely activated over the Brønsted acid sites in HZSM-5, forming some kind of carbenium ions, and that the NO_2 forms NO^+ species, probably situated on Brønsted acid sites. It is conceivable that the carbenium ions and the NO^+ react to form isocyanates, since these species are present at the sample surface. For the acidic sample (HZSM-5 40) at higher temperature (450 °C), NH vibrations are observed (with propane as a reducing agent for NO_2), and it is probable that the isocyanate species are hydrolysed to form some type of amine species.

The reaction between isopropylamine and NO_2 is fast compared with the corresponding reaction with propane. In this reaction the NO^+ species are likely to react with the amine species over Brønsted acid sites. These results indicate that amine species are possible intermediates in the SCR reaction with saturated hydrocarbons as a reducing agent, over acidic zeolites. However, for the reaction to occur the activation of the hydrocarbon, forming some kind of carbenium ions, and the formation of NO^+ species seem to be indispensable.

Acknowledgments

The authors thank Prof. Bengt Andersson, Chalmers University of Technology, for valuable discussions concerning

mass transfer limitations and Albemarle Catalysts BV for providing the zeolites. The KK foundation is kindly acknowledged for financial support via the materials research school (MARCHAL). This work was performed at the Competence Centre for Catalysis, which is hosted by Chalmers University of Technology and financially supported by the Swedish Energy Agency and the member companies: AB Volvo, Johnson Matthey-CSD, Saab Automobile Powertrain AB, Perstorp AB, AVL-MTC AB, Albemarle Catalysts and the Swedish Space Corporation.

Appendix A. Influence of Internal diffusion limitations: Weisz–Prater method

The influence of mass transfer limitations in a porous catalyst can be estimated by calculation of the Weiszs–modulus

$$\Phi = \frac{r_v r_p^2}{D_{eff} c_{as}}, \tag{A.1}$$

where r_v is the reaction rate per volume of the catalyst, r_p is the particle radius, D_{eff} is the effective diffusivity, and c_{as} is the surface concentration of the reactant. The Weisz–Prater criterion can then be used; that is,for an isothermal spherical catalyst particle and a first-order reaction, $\Phi < 1$ indicates a particle free from internal concentration gradients [63].

If the concentration at the surface of the catalyst particle is well approximated with the concentration in the gas bulk, the Weisz modulus may be estimated with the following expression:

$$\Phi = \frac{r_{obs}\rho_{cat} r_p^2}{D_{eff} c_r}.$$

However, for the present case the catalyst particle consists of small zeolite particles, and hence the Weisz-modulus for the small zeolite particles must also be taken into account. The effective diffusivity for the catalyst particle is estimated as $D_{eff,cat.part.} = \varepsilon_p D_{bulk}/3 = 0.35 \times 2 \times 10^{-5}/3 = 2 \times 10^{-6}$ m^2/s, and the effective diffusivity for the zeolite particle ($D_{eff,zeolite.part.}$) is approximately 10^{-11} m^2/s [64,65]. For the zeolite particles the pore volume must be included in the observed reaction rate (r_{obs}); hence $r_{obs,zeolite.part.} = r_{obs}/(1-\varepsilon_p)$. The density of the catalyst (ρ_{cat}) is approximately 600 kg/m^3, the radius of the zeolite particle ($r_{p,zeolite}$) is estimated to be 0.5 μm, and the radius of the catalyst particle ($r_{p,cat}$) is estimated at 250 μm. The concentrations of reactants (c_{NO_2} and $c_{C_3H_8}$) are 18 and 5.1 mmol/m^3, respectively. The observed reaction rates and the estimation of the Weisz modulus are presented in Table A.1.

For all samples the calculated values of the Weiszs modulus are below 1 (see Table A.1); hence the catalytic reaction is likely not influenced by mass transport limitations.

Table A.1
The values used for estimation of the Weisz-modulus at 450 °C

	r_{obs} (mol/(s kg$_{cat}$))	Φ
HZSM-5 40		
$NO_{2\ cat.part.}$	4.0×10^{-4}	0.43
$NO_{2\ zeolite.part.}$	6.1×10^{-4}	0.52
$C_3H_{8\ cat.part.}$	2.1×10^{-4}	0.77
$C_3H_{8\ zeolite.part.}$	3.2×10^{-4}	0.95
HZSM-5 234		
$NO_{2\ cat.part.}$	1.7×10^{-4}	0.18
$NO_{2\ zeolite.part.}$	2.6×10^{-4}	0.23
$C_3H_{8\ cat.part.}$	1.2×10^{-4}	0.44
$C_3H_{8\ zeolite.part.}$	1.8×10^{-4}	0.54
HZSM-5 569		
$NO_{2\ cat.part.}$	1.4×10^{-4}	0.15
$NO_{2\ zeolite.part.}$	2.1×10^{-4}	0.18
$C_3H_{8\ cat.part.}$	3.5×10^{-5}	0.13
$C_3H_{8\ zeolite.part.}$	5.4×10^{-5}	0.16

References

[1] N. Takahashi, H. Shinjoh, T. Iijima, T. Suzuki, K. Yamazaki, K. Yokota, H. Suzuki, N. Miyoshi, S. Matsumoto, T. Tanizawa, T. Tanaka, S. Tateishi, K. Kasahara, Catal. Today 27 (1996) 63.
[2] E. Fridell, M. Skoglundh, B. Westerberg, S. Johansson, G. Smedler, J. Catal. 183 (1999) 196.
[3] E. Fridell, M. Skoglundh, S. Johansson, B. Westerberg, A. Törncrona, G. Smedler, Stud. Surf. Sci. Catal. 116 (1998) 537.
[4] V.I. Parvulescu, P. Grange, B. Delmon, Catal. Today 46 (1998) 233, and references herein.
[5] M. Wallin, C.J. Karlsson, M. Skoglundh, A. Palmqvist, J. Catal. 218 (2003) 354.
[6] M. Wallin, C.-J. Karlsson, A. Palmqvist, M. Skoglundh, Top. Catal. 30/31 (2004) 107.
[7] F. Acke, M. Skoglundh, Appl. Catal. B 22 (1999) L1.
[8] F. Acke, M. Skoglundh, Appl. Catal. B 20 (1999) 235.
[9] F. Acke, M. Skoglundh, Appl. Catal. B 20 (1999) 133.
[10] F. Acke, B. Westerberg, L. Eriksson, S. Johansson, M. Skoglundh, E. Fridell, G. Smedler, Stud. Surf. Sci. Catal. 116 (1998) 285.
[11] F. Acke, B. Westerberg, M. Skoglundh, J. Catal. 179 (1998) 528.
[12] R. Burch, A.A. Shestov, J.A. Sullivan, J. Catal. 182 (1999) 497.
[13] R. Burch, J.A. Sullivan, J. Catal. 182 (1999) 489.
[14] R. Burch, T.C. Watling, J. Catal. 169 (1997) 45.
[15] R. Burch, P.J. Millington, Catal. Today 26 (1995) 185.
[16] H. Hamada, Catal. Today 22 (1994) 21.
[17] G. Zhang, T. Yamaguchi, H. Kawakami, T. Suzuki, Appl. Catal. B 1 (1992) L15.
[18] H. Hattori, O. Takahashi, M. Takagi, K. Tanabe, J. Catal. 68 (1981) 132.
[19] M. Hino, K. Arata, Catal. Lett. 30 (1995) 25.
[20] R. Burch, E. Halpin, M. Hayes, K. Ruth, J.A. Sullivan, Appl. Catal. B 19 (1998) 199.
[21] C.P. Hubbard, K. Otto, H.S. Gandhi, K.Y.S. Ng, Catal. Lett. 30 (1995) 41.
[22] A.F. Lee, K. Wilson, R.M. Lambert, C.P. Hubbard, R.G. Hurley, R.W. McCabe, H.S. Gandhi, J. Catal. 184 (1999) 491.
[23] M. Skoglundh, A. Ljungqvist, M. Petersson, E. Fridell, N. Cruise, O. Augustsson, E. Jobson, Appl. Catal. B 30 (2001) 315.
[24] K. Wilson, C. Hardacre, R.M. Lambert, J. Phys. Chem. 99 (1995) 13755.
[25] H.C. Yao, H.K. Stephen, H.S. Gandhi, J. Catal. 67 (1981) 231.
[26] H.H. Ingelsten, M. Skoglundh, E. Fridell, Appl. Catal. B 41 (2003) 287.

[27] H.H. Ingelsten, Å. Hildesson, E. Fridell, M. Skoglundh, J. Mol. Catal. A 209 (2004) 199.
[28] J.A. Martens, A. Cauvel, F. Jayat, S. Vergne, E. Jobson, Appl. Catal. B 29 (2001) 299.
[29] T. Holma, A. Palmqvist, M. Skoglundh, E. Jobson, Appl. Catal. B 48 (2004) 95.
[30] A. Hinz, M. Skoglundh, E. Fridell, A. Andersson, J. Catal. 201 (2001) 247.
[31] K. Hadjiivanov, J. Saussey, J.L. Freysz, J.C. Lavalley, Catal. Lett. 52 (1998) 103.
[32] J. Szanyi, M.T. Paffett, J. Catal. 164 (1996) 232.
[33] M. Trombetta, G. Busca, S. Rossini, V. Piccoli, U. Cornaro, A. Guercio, R. Catani, R.J. Willey, J. Catal. 179 (1998) 581.
[34] G. Boskovic, T. Vulic, E. Kis, P. Putanov, Chem. Eng. Technol. 24 (2001) 269.
[35] F. Poignant, J.L. Freysz, M. Daturi, J. Saussey, Catal. Today 70 (2001) 197.
[36] B.I. Mosqueda-Jimenez, A. Jentys, K. Seshan, J.A. Lercher, Appl. Catal. B 43 (2003) 105.
[37] P.E. Fanning, M.A. Vannice, J. Catal. 207 (2002) 166.
[38] E.H. Teunissen, R.A. Vansanten, A.P.J. Jansen, F.B. Vanduijneveldt, J. Phys. Chem. 97 (1993) 203.
[39] Q. Sun, Z.X. Gao, B. Wen, W.M.H. Sachtler, Catal. Lett. 78 (2002) 1.
[40] R. Szostak, Molecular Sieves, Van Nostrand Reinhold, New York, 1989.
[41] J. Eng, C.H. Bartholomew, J. Catal. 171 (1997) 27.
[42] M. Xin, I.C. Hwang, S.I. Woo, J. Phys. Chem. B 101 (1997) 9005.
[43] K.I. Hadjiivanov, Catal. Rev.-Sci. Eng. 42 (2000) 71.
[44] S.A. Beloshapkin, E.A. Paukshtis, V.A. Sadykov, J. Mol. Catal. A 158 (2000) 355.
[45] A. Obuchi, C. Wogerbauer, R. Koppel, A. Baiker, Appl. Catal. B 19 (1998) 9.
[46] H.Y. Chen, T. Voskoboinikov, W.M.H. Sachtler, J. Catal. 180 (1998) 171.
[47] H.Y. Chen, T. Voskoboinikov, W.M.H. Sachtler, Catal. Today 54 (1999) 483.
[48] M. Yamaguchi, J. Chem. Soc.-Faraday Trans. 93 (1997) 3581.
[49] F. Solymosi, T. Bansagi, J. Catal. 156 (1995) 75.
[50] S.K. Park, H. Choo, L. Kevan, Phys. Chem. Chem. Phys. 3 (2001) 3247.
[51] H.Y. Chen, T. Voskoboinikov, W.M.H. Sachtler, J. Catal. 186 (1999) 91.
[52] T. Shimanouchi, in: Tables of Molecular Vibrational Frequences Consolidated, vol. 1, National Bureau of Standards, Washington, 1972, pp. 1–160.
[53] F. Poignant, J. Saussey, J.C. Lavalley, G. Mabilon, Catal. Today 29 (1996) 93.
[54] S.K. Park, Y.K. Park, S.E. Park, L. Kevan, Phys. Chem. Chem. Phys. 2 (2000) 5500.
[55] R. Burch, J.P. Breen, F.C. Meunier, Appl. Catal. B 39 (2002) 283.
[56] I.O.Y. Liu, N.W. Cant, B.S. Haynes, P.F. Nelson, J. Catal. 203 (2001) 487.
[57] R. Brosius, J.A. Martens, Top. Catal. 28 (2004) 119.
[58] NIST Standard Reference Database 69, Coblentz No. 8753, http://webbook.nist.gov/chemistry/ (18 October, 2004).
[59] P. Svedberg, E. Jobson, S. Erkfeldt, B. Andersson, M. Larsson, M. Skoglundh, Top. Catal. 30–31 (2004) 199.
[60] F.C. Jentoft, B.C. Gates, Top. Catal. 4 (1997) 1.
[61] A.D. Cowan, R. Dumpelmann, N.W. Cant, J. Catal. 151 (1995) 356.
[62] A.D. Cowan, N.W. Cant, B.S. Haynes, P.F. Nelson, J. Catal. 176 (1998) 329.
[63] P.B. Weiszs, C.D. Prater, Adv. Catal. 6 (1954) 143.
[64] S.F. Garcia, P.B. Weisz, J. Catal. 142 (1993) 691.
[65] A.S. Chiang, A.G. Dixon, Y.H. Ma, Chem. Eng. Sci. 39 (1984) 1461.